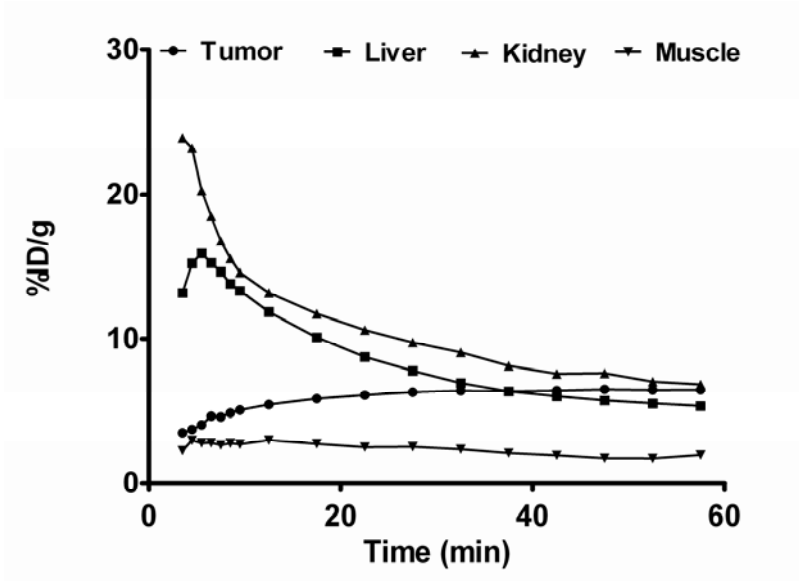
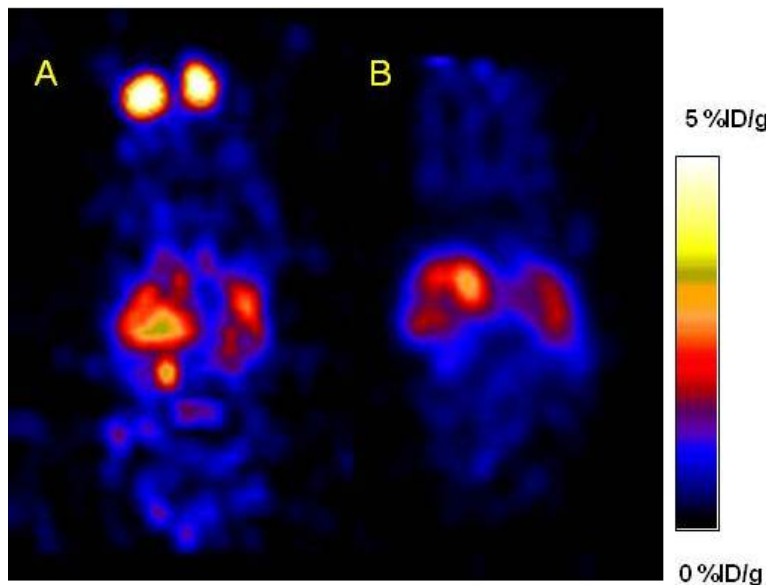


**Supplemental Figure 1.** *In vivo* biodistribution of  $^{18}\text{F}$ -FBZA in B16F10, A375M and U87MG tumor bearing mice and  $^{18}\text{F}$ -FDG in B16F10 tumor bearing mice. Data are expressed as the percentage administered activity (injected dose) per gram of tissue (%ID/g) after intravenous injection of  $^{18}\text{F}$ -FBZA or  $^{18}\text{F}$ -FDG (100  $\mu\text{Ci}$ ) at designated time points (n = 3 for each group). **(A)**  $^{18}\text{F}$ -FBZA uptake in %ID/g. **(B)**  $^{18}\text{F}$ -FBZA tumor-to-organ ratios. **(C)**  $^{18}\text{F}$ -FDG uptake in %ID/g. **(D)**  $^{18}\text{F}$ -FDG tumor-to-organ ratios (T represents for Tumor).



**Supplemental Figure 2.** *In vivo* biodistribution of intravenously injected  $^{18}\text{F}$ -FBZA measured by using ROI analysis of dynamic small-animal PET data sets in C56BL/6 mice bearing B16F10 tumors ( $n = 3$ ). Rapid uptake and clearance of  $^{18}\text{F}$ -FBZA were observed in both liver and kidney. Rapid tumor uptake and sustained retention for the probe was also found. Error bars were omitted for better visibility.



**Supplemental Figure 3.** Representative decay-corrected coronal small-animal  $\mu\text{PET}$  images of  $^{18}\text{F}$ -FBZA in eyes of C57BL/6 (A) vs. nude mouse (B). Eyes lit up in C57BL/6 mouse.